MDPI

Article

Regulating Monolayer Aligned Silver Nanowire Coatings for Energy-Saving Windows

Zhongrui Yu [1], Huirong Ma [2], Yuqiu Shao [1], Xiaole Yu [2], Jingjing Chen [1], Chenlong Dong [1,*], Zhiyong Mao [2] and **Dajian Wang [2,*]**

[1]   Tianjin Key Laboratory for Photoelectric Materials and Devices, School of Materials Science and Engineering, Tianjin University of Technology, Tianjin 300384, China

[2]   Key Laboratory of Display Materials and Photoelectric Devices, Tianjin University of Technology, Ministry of Education, Tianjin 300384, China

*   Correspondence: dongchenlong@email.tjut.edu.cn (C.D.); djwang@tjut.edu.cn (D.W.)

Abstract: Low-emissivity (low-e) glass has garnered considerable attention for implementation in energy-saving windows, which can effectively decrease the energy consumption of buildings. However, the traditional vacuum-coating technology of low-e films greatly enhances the cost of energy-saving windows, and the influence of the vacuum-coating parameters on the optical characteristics of low-e films necessitates a complex optimization process. Herein, we prepared Ag NWs with controllable diameters using the polyol method, and the alignment of the Ag NW film coating on glass substrates was regulated by the shear force of the liquid flow generated through magnetic stirring. After optimization, the low-ε_{MIR} windows based on aligned Ag NW (60 nm) coatings showed an optical transmittance of 84.4% and a low ε_{MIR} of 0.3, which were superior to those of commercial low-ε_{MIR} glass (T: 65.6%; ε_{MIR}: 0.4). The simplicity and low cost of aligned Ag NW coatings for low-e glass open up a new avenue for reducing energy consumption in existing windows.

Keywords: energy-saving window; silver nanowire coating; orientation alignment; optical transmittance; low-emissivity

1. Introduction

In recent years, more than thirty percent of global energy consumption has been attributed to buildings [1], and HVAC (heating, ventilation, and air conditioning) systems in residential and commercial buildings account for the majority of this energy consumption [2,3]. Approximately one third of the energy loss from a typical house comes from the windows, due to their high optical transmittance and thermal radiation [4–7]. Therefore, in order to decrease the energy consumption of buildings, low-emissivity windows must be developed.

Low thermal radiation and high visible transmittance are attractive characteristics of low-emissivity windows. So far, various functional materials, such as metal-based multilayer coatings [8,9] and doped semiconductors with broad band gaps [10–13], have been employed for low-emissivity (low-e) films [14]. Due to its relatively low absorption in the visible light region and high reflectance in the IR region [8], Ag is a promising material for energy-saving windows. However, the use of vacuum-coating technology is severely constrained by the exceedingly high cost and difficult processing requirements. Accordingly, it is essential to develop a low-emissivity material that can be applied in a straightforward manner while maintaining the functionality of low-e films. Recently, Yu et al. fabricated energy-saving smart windows through the high-efficiency spray assembly of thermos plasmonic gold nanoparticles (Au NPs) [15]. Such methods for fabricating low-emissivity windows are relatively simple, but Au NPs are more expensive than Ag NPs.

Ag nanowire (NW) networks, characterized by 1D properties, high visible-light transmittance, and a straightforward manufacturing method, can reflect back IR radiation to

prevent heat loss and have therefore been employed in personal thermal management [16]. Motivated by this, Ag NWs ought to be a candidate nanostructured Ag material for low-e windows [17,18]. Due to its simplicity and usefulness, the direct spray coating of random Ag NWs on glass has been exploited for depositing traditional Ag NW coatings on energy-saving windows [19,20]. However, the transmittance is inevitably influenced by the random network of Ag NWs [21], partially due to the uncontrolled interwire spacings. However, regulating the interwire spacings to ensure the regular arrangement of Ag NWs is largely dependent on the size of the Ag NWs and the coating technology.

Herein, Ag NWs of different diameters were prepared via the $CuCl_2$-mediated polyol method by adjusting the content of the KBr template. Then, relying on the shear force of the liquid flow generated through magnetic stirring, orientation-aligned Ag NWs were coated onto SiO_2 glass, and the interwire spacings were easily controlled according to the stirring duration. After optimization, the energy-saving window with a Ag NW interval distance of 0.68 μm demonstrated a low emissivity in the mid-infrared region (ε_{MIR}) of 0.3 and an optical transmittance (T) of 84.4%. This stirring-assisted orientation alignment strategy could pave the way for a new coating technology for low-e energy-storage windows.

2. Materials and Methods

Silver nitrate ($AgNO_3$, AR) was purchased from Tianjin YingDa Chemical Reagents Co., Ltd. (Tianjin, China). Copper chloride ($CuCl_2$ $2H_2O$, AR); polyvinylpyrrolidone (PVP, M_w = 58,000); and polyvinyl butyral (PVB, M_w = 170,000–250,000) were purchased from Macklin. Ethylene glycol (EG, 99.5%); ethanol (99.7%); and potassium bromide (KBr, AR) were purchased from Tianjin FuChen Chemical Reagents Co., Ltd. (Tianjin, China). Glass substrates (24 mm × 24 mm × 1 mm) were purchased from GuLuo Glass Co., Ltd. (Luoyang, China). Deionized water was prepared using a UPT ultrapure water dispenser (UPT-II-20T, Chengdu Chaochun Technology Co., Ltd., Chengdu, China). The suppliers and purity of the materials are listed in Table 1. All chemicals in this work were used without further purification.

Table 1. The suppliers and purity of the materials.

Material	Supplier	Purity
$AgNO_3$	Tianjin YingDa Chemical Reagents Co., Ltd. (Tianjin, China)	AR
$CuCl_2.2H_2O$	Shanghai Macklin Biochemical Co. Ltd. (Shanghai, China)	AR
PVP, Mw = 58,000	Shanghai Macklin Biochemical Co. Ltd. (Shanghai, China)	AR
PVB, Mw = 170,000–250,000	Shanghai Macklin Biochemical Co. Ltd. (Shanghai, China)	AR
EG	Tianjin FuChen Chemical Reagents Co., Ltd. (Tianjin, China)	99.5%
Ethanol	Tianjin FuChen Chemical Reagents Co., Ltd. (Tianjin, China)	99.7%
KBr	Tianjin FuChen Chemical Reagents Co., Ltd. (Tianjin, China)	AR
Deionized water	UPT-II-20T, Chengdu Chaochun Technology Co., Ltd. (Chengdu, China)	Resistivity = 18.2 MΩ cm

Synthesis of Ag NWs: Generally, 0.66 g of PVP was dissolved in 50 mL EG under magnetic stirring at 80 °C. Then, 1 mL 0.01 M $CuCl_2$/EG solution and 0.25–1 mL 0.01 M KBr/EG solution were rapidly injected into the PVP/EG solution. Subsequently, 3.2 mmol $AgNO_3$ powder was instilled into the above solution under magnetic stirring, and the color changed from colorless to saffron yellow. The mixture was kept in an oven at 145 °C for 4 h. After cooling down to room temperature, the resultant solution was set for two days. The resultant Ag NWs were separated by centrifugation at 2000 rpm and washed several times using deionized water and ethanol. Finally, the clean Ag NWs were redispersed in 100 mL ethanol for further characterization.

Preparation of energy-saving nanowire films with different interwire spacings: Ag NW films with different interwire spacings were fabricated by the stirring-assisted orientation alignment strategy [16]. The experiment was performed using a common laboratory magnetic stirrer. First, SiO_2 glass substrates (24 mm × 24 mm × 1 mm) were sonicated in

deionized water and ethanol for 20 min to remove the impurities on the glass surface. The as-cleaned glass substrates were treated with ozone for 20 min. The ozone-treated glass substrates were fixed to the inner wall of a beaker containing 60 mL 1 mg mL^{-1} Ag NWs in the PVB solution (1 wt.%). The solution was stirred at 400 rpm for 0.5–2 h, and finally the glass substrates were dried under N_2 flow.

The crystal structures of the Ag NWs were investigated by X-ray diffraction (XRD) using an ARL EQUINOX 3000 X-ray diffractometer (Thermo Fisher Scientific, Waltham, MA, USA) with Cu Kα radiation (λ = 1.5418 Å) in the 2θ range of 10–90°. The morphologies of the Ag NWs were measured by a scanning electron microscope (SEM) with a field emission gun (Quanta FEG 250, FEI, Hillsboro, OR, USA). Transmission electron microscopy (TEM) using a Talos F200× (FEI, Hillsboro, OR, USA) microscope was performed to observe the morphology, microstructure, and composition. UV–vis spectra were collected by a Lambda 750 (PerkinElmer, Waltham, MA, USA) spectrophotometer. The transmittance and haze factors were measured with the Lambda 750 (PerkinElmer, Waltham, MA, USA) spectrophotometer using the standard test method (Haze ASTM D-1003-00). The mid-IR emissivity and mid-IR reflectivity of the Ag NWs were measured by a FTIR spectrometer (Frontier Mid-IR FTIR/STA6000-TL9000-Clarus SQ8, PerkinElmer, Waltham, MA, USA). The IR images were taken with an IR camera (InfiRay C210, Hunan, China). The nomenclature involving in the text is listed in Table 2.

Table 2. Nomenclature.

Abbreviation	Meaning
T	Transmittance
R	Reflectance
ε_{MIR}	Emissivity of mid-infrared region
XRD	X-ray diffraction
SEM	Scanning electron microscope
TEM	Transmission electron microscope
FTIR spectrometer	Fourier transform infrared spectrometer
UV–Vis	UV-visible spectrophotometer

3. Results and Discussion

Ag NWs with different diameters were prepared using the $CuCl_2$-mediated polyol method by adjusting the addition of KBr templates, as illustrated in Figure 1a. Firstly, the Ag^+ combined with the Cl^- from the $CuCl_2$ to form AgCl colloids, effectively decreasing the concentration of Ag^+ (aq). Then, at 145 °C, the Cu^{2+} was reduced to Cu^+, which depleted the dissolved oxygen and adsorbed oxygen at the surface of the Ag NWs, thus avoiding the formation of Ag nanoparticles [22]. Moreover, the addition of an extra KBr template increased the number of five-fold twin crystals in the initial period of the reaction, which produced a smaller crystal seed and thus decreased the diameter of the Ag NWs [23]. When the amount of KBr was 0.25 mL, the average diameter of the Ag NWs was 88 nm (Figure 1b). With the amount of KBr increasing from 0.5 to 1 mL, the average diameter of the Ag NWs reduced from 70 to 47 nm (Figure 1c–e), accompanied by the formation of some by-products (AgBr nanoparticles) (Figure 2). The formation of AgBr nanoparticles could have been due to the addition of too much Br^-, covering all the crystal faces of the multiple twins and hindering the deposition of silver atoms on the (111) planes of the five-fold twin crystals [24].
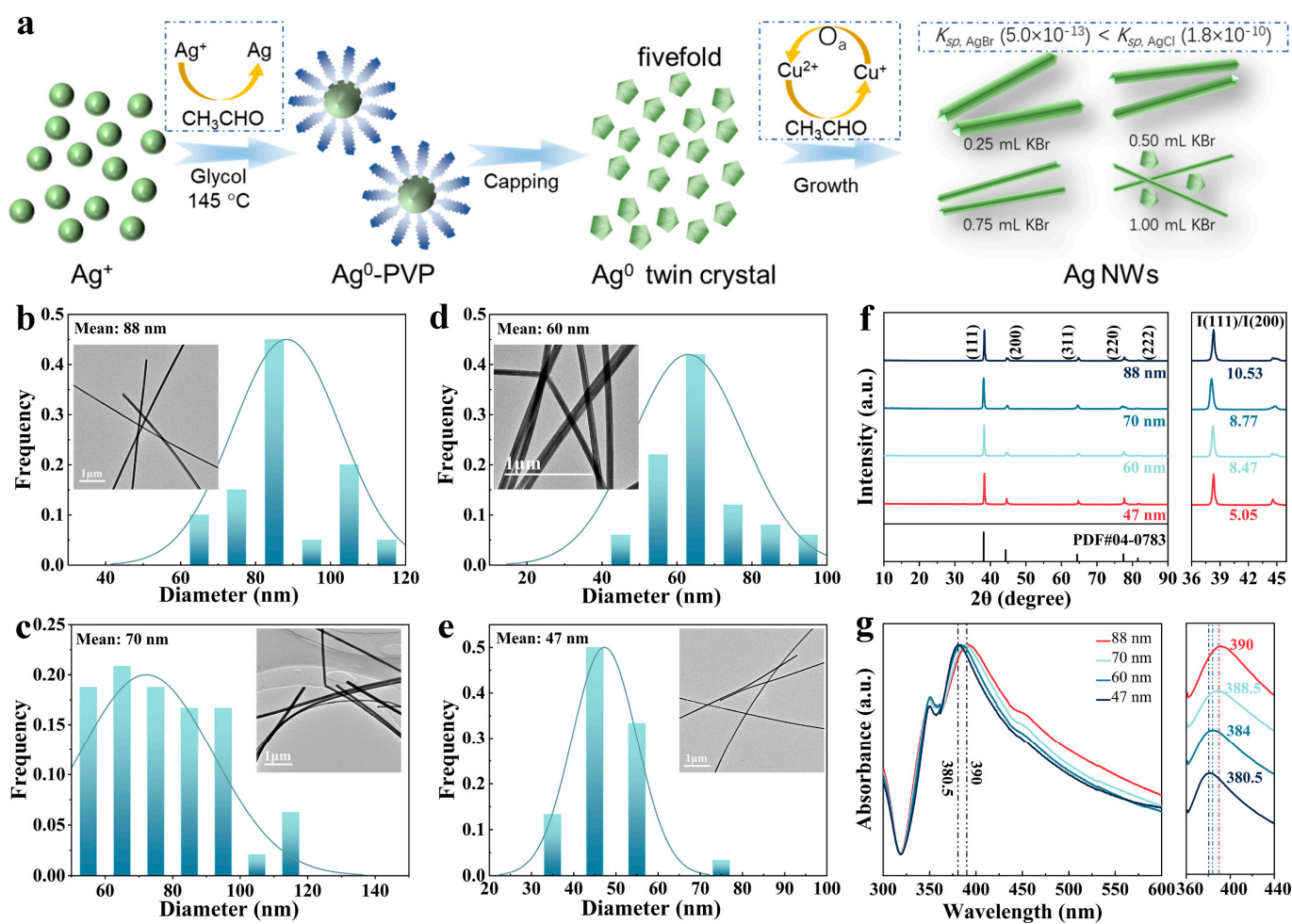
Figure 1. (**a**) Schematic illustration of the synthesis of Ag NWs. The diameter distributions of the Ag NWs synthesized with different amounts of Br^- were: (**b**) 0.25 mL; (**c**) 0.5 mL; (**d**) 0.75 mL; and (**e**) 1 mL. Insets: TEM images of the corresponding Ag NWs. (**f**) XRD patterns and (**g**) UV-Vis spectra of the Ag NWs with different diameters.
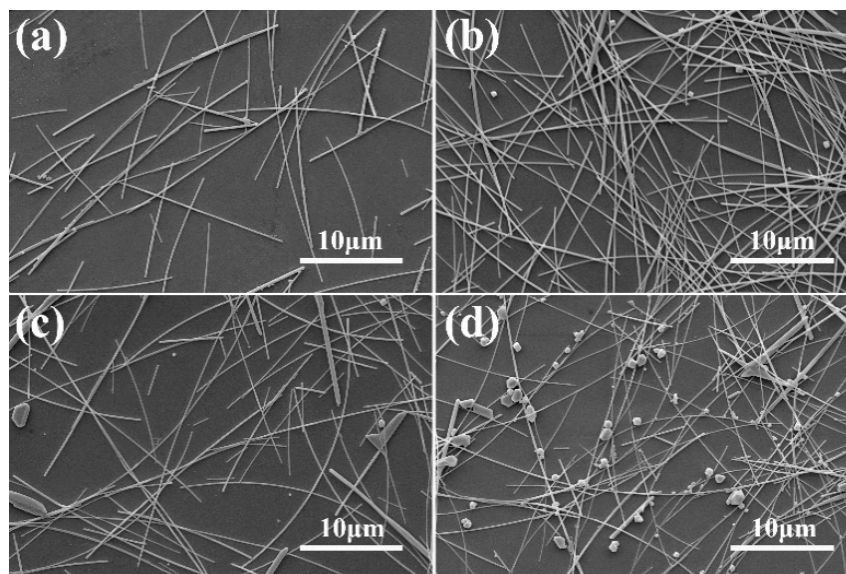

Figure 2. SEM of Ag NWs with diameters of (**a**) 88 nm, (**b**) 70 nm, (**c**) 60 nm, and (**d**) 47 nm.

To investigate the crystal phase and phase purity, the XRD of Ag NWs with different diameters was carried out, as shown in Figure 1f. The characteristic peaks of the Ag NWs at 11.8°, 16.8°, 26.7°, and 55.9° could be indexed as the (111), (200), (220), and (311) planes of Ag (JCPDF #04-0783), respectively. No other impurity peaks were observed, suggesting the high phase purity of the as-synthesized Ag NWs. Moreover, with the amount of Br$^-$ increasing, the $I_{(111)}/I_{(200)}$ decreased from 10.53 to 5.05, which revealed the decreased diameter of the obtained Ag NWs. The theoretical $I_{(111)}/I_{(200)}$ for cubic Ag is 2.5, which is much lower than that of the Ag NWs, demonstrating the predominant (111) orientation of the Ag NWs [25]. Taking the Ag NWs with a diameter of 60 nm as an example, transmission electron microscopy (TEM) was performed to check the microstructure along with the crystal selectivity (Figure 3). The lattice spacing of 0.237 nm on the top region of the Ag NWs could be attributed to the (111) plane of Ag (Figure 3b). The SAED pattern further confirmed the existence of single-crystal Ag NWs, and the (111), (100), (110), (311) planes could be checked in accordance with the HRTEM and XRD results.
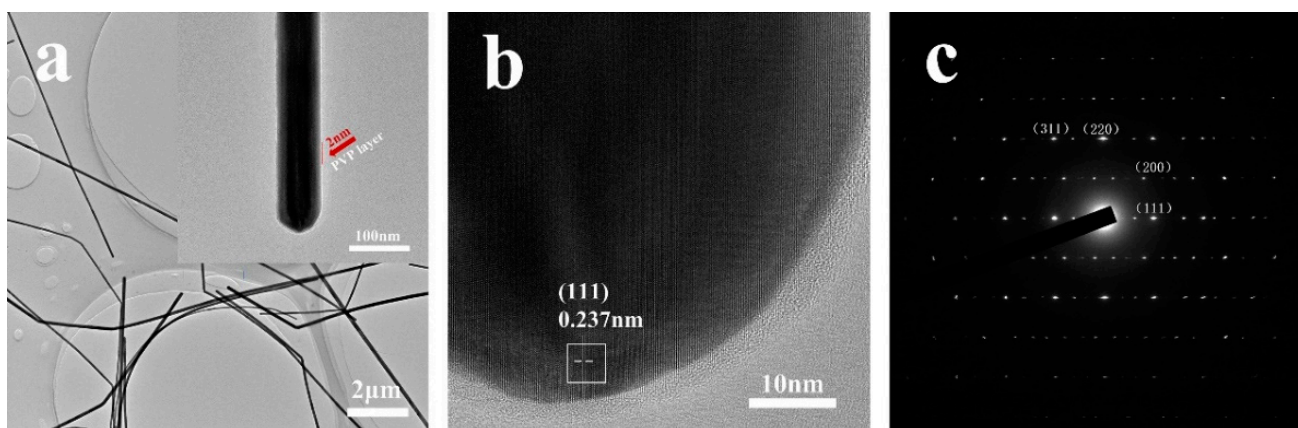

Figure 3. (**a**) Low-resolution TEM, (**b**) high-resolution TEM, and (**c**) SAED images of Ag NWs with an average diameter of 60 nm.

To better comprehend the absorption characteristics of the Ag NWs, we obtained UV–vis absorption spectra with a wavelength ranging from 300 to 600 nm. When the amount of Br$^-$ was 0.25 mL, the UV–Vis spectra showed an absorption peak at ca. 390 nm with a small shoulder peak at 350 nm, both of which could be attributed to the transversal surface plasmon resonance (SPR) modes of the Ag nanowires with pentagonal cross-sections [26]. The absence of the strong peak at 430 nm in the Ag nanoparticles indicated the purity of the Ag nanowires [27]. With the amount of Br$^-$ increasing from 0.25 to 1 mL, the SPR peaks displayed a continuous blue shift from 390 to 380.5 nm, partially due to the decreased diameter of the Ag NWs [28].

For the practical experiment, we adopted the as-synthesized Ag NWs with a diameter of 60 nm as building blocks to fabricate an energy-saving window, using the shear force of the liquid flow generated through magnetic stirring to align the NWs. The cleaned SiO$_2$ glass substrates were treated by UV ozone to ensure good hydrophilicity. The results of the contact angle measurements (Video S1, see Supplementary Materials) showed that the hydrophilicity of the substrate was greatly increased. These glass substrates were fixed to the inner wall of a beaker containing a Ag NW suspension. The liquid flow direction was maintained in the same direction as the shear force, and the Ag NWs in suspension aligned in the same direction as the liquid flow, as illustrated in Figure 4a.
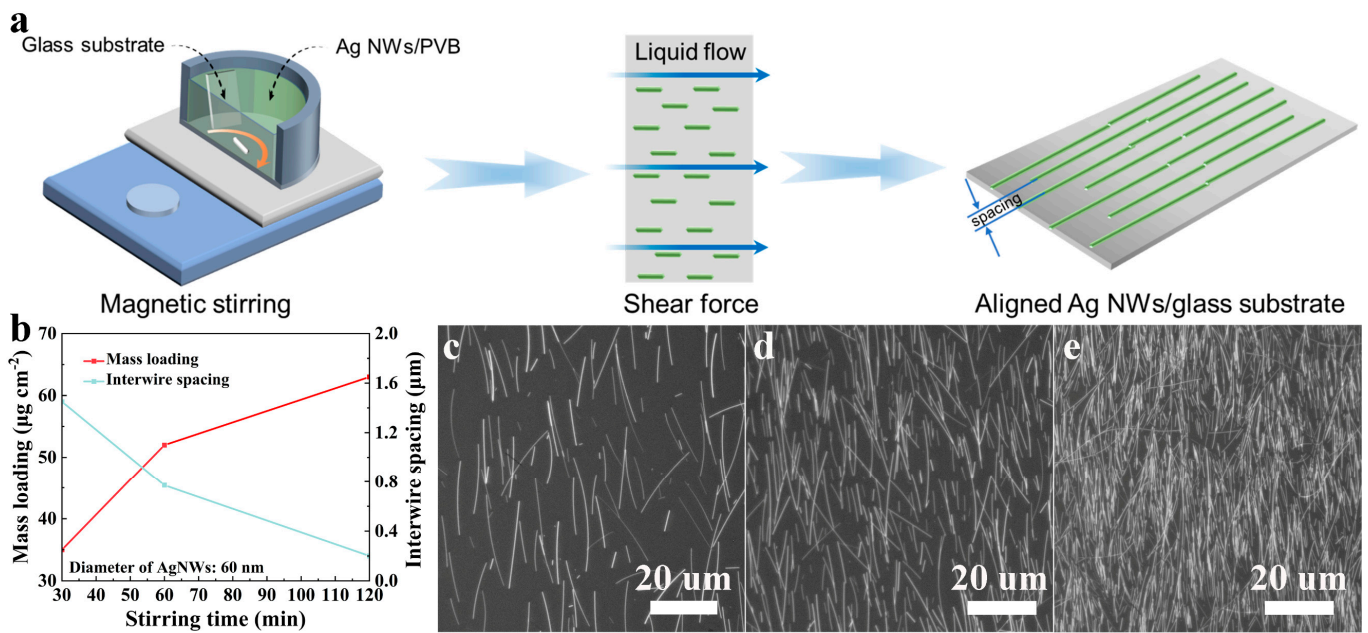
Figure 4. (**a**) Schematic illustration of stirring-assisted orientation alignment of Ag NWs. (**b**) Influence of the stirring duration on mass loading and interwire spacing of Ag NWs. SEM images of aligned Ag NWs with average interwire spacings of (**c**) 1.36 μm, (**d**) 0.68 μm, and (**e**) 0.28 μm.

Theoretically, the mass loading of the Ag NWs was positively correlated with the duration of the shear force application on the glass substrates. Thus, the interwire spacings could be easily controlled by the stirring time (Figures 4b and 5). The mass loading of the Ag NWs on the glass substrate increased from 35 to 63 μg cm^{-2} as the stirring time increased from 30 min to 120 min. As is evident from the optical microscopy images in Figure 4c–e, the shear forces generated by high-speed stirring mediated the directional movement of the Ag NWs and finally induced the regular alignment of the Ag NWs on the glass substrate. The interwire spacings of the Ag NWs decreased from 1.36 μm to 0.28 μm with an increase in the stirring times from 30 min to 120 min.
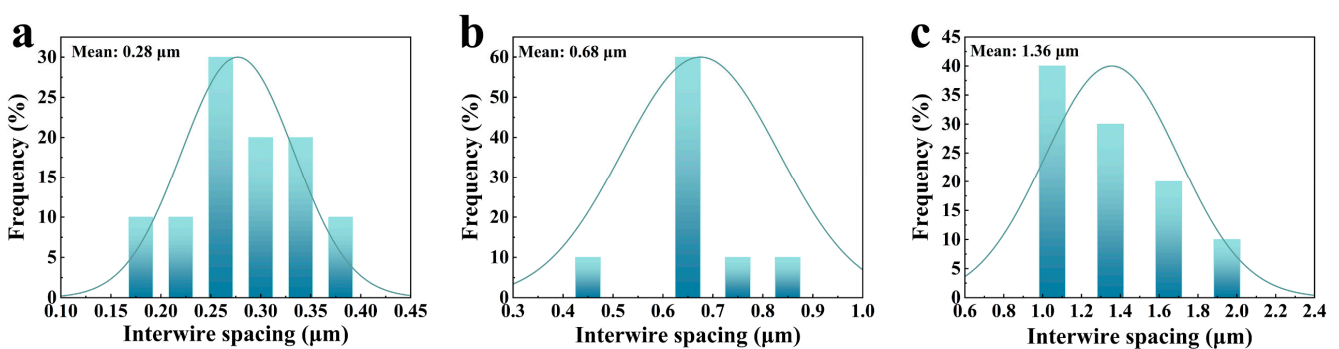

Figure 5. The interwire spacing distribution of 60 nm Ag NWs with stirring times of (**a**) 120 min, (**b**) 90 min, and (**c**) 30 min.

To accurately evaluate the characteristics and performance of the aligned Ag NW-coated energy-saving windows, the side coated with the aligned Ag NWs faced towards the inside. The mechanism of the aligned Ag NW-based energy-saving windows is shown in Figure 6a. The glass can transmit most visible light and reduce the heat transfer from indoors to outdoors, because a large proportion of the thermal radiation in the MIR range can be reflected. Figure 6b shows the transmittance spectra of the Ag NW films with different interwire spacings in the wavelength range of 400–600 nm. The transmittance (T) at 550 nm decreased from 89.2% to 82.2% as the interwire spacings of the Ag NWs

decreased from 1.36 to 0.28 µm. This decreased T of the Ag NW films with smaller interwire spacings could be attributed to the increased mass loading of the Ag NWs.
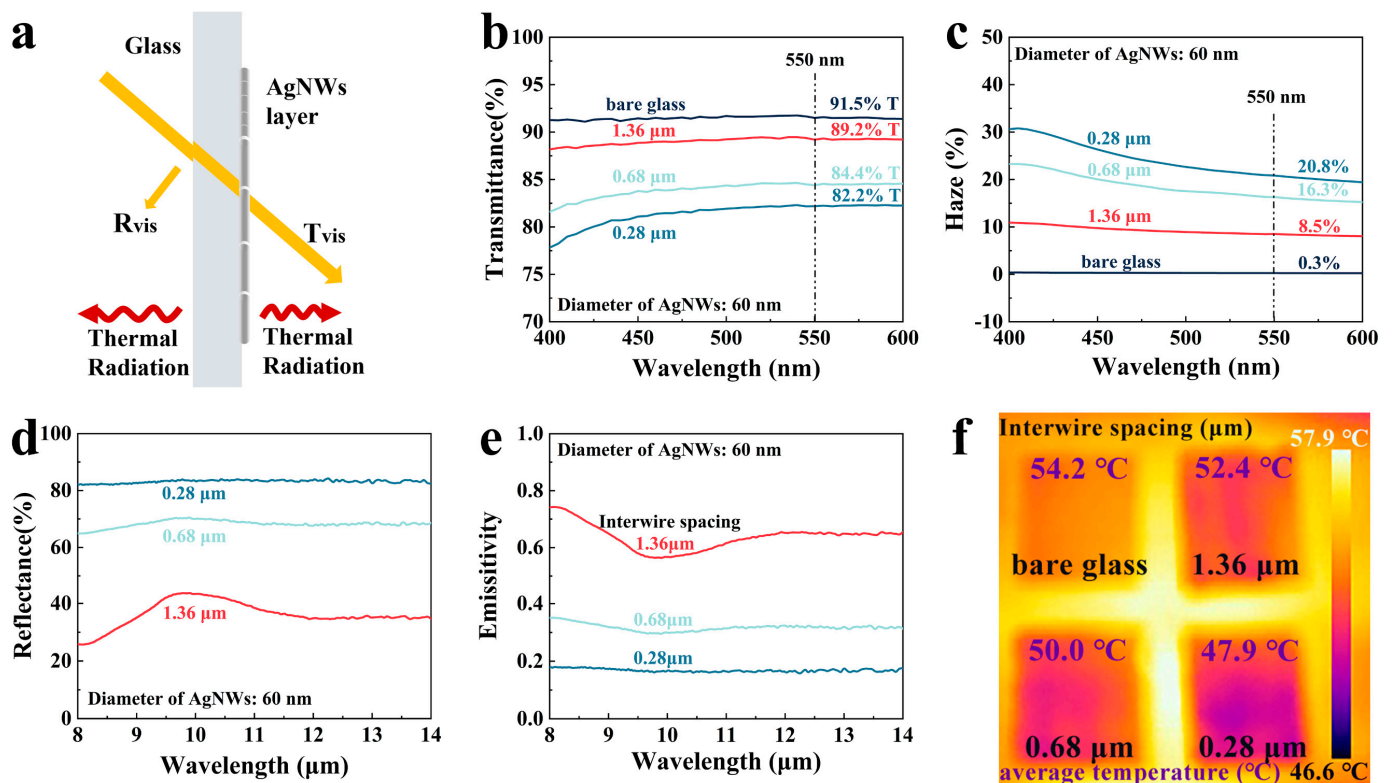

Figure 6. (**a**) Schematic illustration of the energy-saving windows coated with one layer of aligned silver nanowires. (**b**) Transmittance, (**c**) haze factor, (**d**) reflectance, and (**e**) emissivity of the aligned silver nanowires with different interwire spacings. (**f**) Heat-insulating performance of the bare glass and the aligned silver nanowires with different interwire spacings.

Haze is another significant parameter for evaluating the performance of energy-saving windows. The haze values for the energy-saving windows covered by Ag NW films with interwire spacings of 0.28, 0.68, and 1.36 µm were 21, 15, and 9%, respectively (Figure 6c). Figure 6d shows the reflectance spectra of the Ag NWs films. There were clear differences between the experimental samples. The reflectance of the films gradually increased from 43% to 82% with the decrease in interwire spacing. Based on the measured reflectance (R) and transmittance (T), the emissivity (ε_{MIR}) of the films could be calculated using the following equation: $\varepsilon_{MIR} = 1 - R - T$. The emissivity of the films gradually decreased from 0.57 to 0.18 with the decrease in interwire spacing (Figure 6e). The energy-saving window with the Ag NW interval distance of 0.68 µm demonstrated a low emissivity in the mid-infrared region (ε_{MIR}) of 0.3 and an optical transmittance (T) of 84.4%, which were superior to those of commercial low-ε_{MIR} glass (T: 65.6%; ε_{MIR}: 0.4).

In order to investigate the low-emissivity properties of the Ag NW films, a heat-insulation performance evaluation was carried out by setting Ag NW-coated glass substrates and a blank glass substrate on a heating plate preheated to 60 °C. The surface temperature was monitored after thermal equilibrium using an infrared thermal imager. As displayed in Figure 6f, the colors of the substrate surfaces ranged from light to dark, corresponding to decreased emissivity. The average temperatures for bare glass and glass substrates coated with Ag NWs with interwire spacings of 0.28, 0.68, and 1.36 µm were 54.2, 52.4, 50.0, and 47.9 °C, respectively. Compared with the bare glass, the temperature of the modified glass substrate was reduced by a maximum of 11.6%, indicating that the emissivity of the Ag NW films was much lower than that of bare glass, which was consistent with the transmittance and reflectivity results.

4. Conclusions

Traditional commercial low-e windows are fabricated by the vacuum coating of metals (silver etc.). This technique requires sophisticated and expensive equipment, which limits its widespread application. In conclusion, by generating shear force through the stirring of the liquid, Ag NWs with different diameters could be regularly aligned on the glass substrates. The interwire spacings of the Ag NWs ranging from 0.28 to 1.36 μm could be controlled by adjusting the stirring time. Benefitting from the optimization of the Ag NW interwire spacing and diameter, the energy-saving windows coated by the aligned Ag NWs with an interwire spacing of 0.68 μm demonstrated a high optical transmittance (84.4%), a high R_{MIR} (70%), and a low ε_{MIR} (0.3), which were comparable to those of commercial low-ε_{MIR} glass (T: 65.6%; ε_{MIR}: 0.4). As a result, the aligned Ag NW-based energy-saving windows displayed a remarkable heat-insulating performance. Such functional Ag NW coatings with highly regular alignments could break new ground in modified energy-saving windows.

Supplementary Materials: The following are available online at https://www.mdpi.com/article/10.3390/coatings12101552/s1, Video S1: The contact angle of water on UV-treated glass.

Institutional Review Board Statement: Not applicable.

Informed Consent Statement: Not applicable.

Data Availability Statement: Data sharing is not applicable to this article.

Conflicts of Interest: The authors declare no conflict of interest.

References

1. Li, T.; Zhai, Y.; He, S.M.; Gan, W.T.; Wei, Z.Y.; Heidarinejad, M.; Dalgo, D.; Mi, R.Y.; Zhao, X.P.; Song, J.W.; et al. A radiative cooling structural material. *Science* **2019**, *364*, 760–763. [CrossRef] [PubMed]
2. Zhao, H.X.; Magoules, F. A review on the prediction of building energy consumption. *Renew Sustain. Energy Rev.* **2012**, *16*, 3586–3592. [CrossRef]
3. Perez-Lombard, L.; Ortiz, J.; Pout, C. A review on buildings energy consumption information. *Energy Build.* **2008**, *40*, 394–398. [CrossRef]
4. Yang, H.J.; Geng, L.; Zhang, Y.T.; Chang, G.; Zhang, Z.L.; Liu, X.; Lei, M.; He, Y.B. Graphene-templated synthesis of palladium nanoplates as novel electrocatalyst for direct methanol fuel cell. *Appl. Surf. Sci.* **2019**, *466*, 385–392. [CrossRef]
5. Wang, X.T.; Cui, Y.; Li, T.; Lei, M.; Li, J.B.; Wei, Z.M. Recent Advances in the Functional 2D Photonic and Optoelectronic Devices. *Adv. Opt. Mater.* **2019**, *7*, 1801274. [CrossRef]
6. Hoffmann, S.; Lee, E.S.; Clavero, C. Examination of the technical potential of near-infrared switching thermochromic windows for commercial building applications. *Sol. Energy Mat. Sol. Cells* **2014**, *123*, 65–80. [CrossRef]
7. Xu, X.D.; Cortie, M.B.; Stevens, M. Effect of glass pre-treatment on the nucleation of semi-transparent gold coatings. *Mater. Chem. Phys.* **2005**, *94*, 266–274. [CrossRef]
8. Martin-Palma, R.J.; Vazquez, L.; Martinez-Duart, J.M.; Malats, R. Silver-based low-emissivity coatings for architectural windows: Optical and structural properties. *Sol. Energy Mat. Sol. Cells* **1998**, *53*, 55–66. [CrossRef]
9. Wu, J.Y.; Qian, X.H.; Liu, C.Y.; Ji, Y.L.; Yu, S.W. Design and realization of neutral-tinted low-E film. *Vacuum* **2022**, *203*, 111228. [CrossRef]
10. Deng, Z.S.; Wang, J.; Wu, A.M.; Shen, J.; Zhou, B. High strength SiO_2 aerogel insulation. *J. Non-Cryst. Solids* **1998**, *225*, 101–104. [CrossRef]
11. Schaefer, C.; Brauer, G.; Szczyrbowski, J. Low emissivity coatings on architectural glass. *Surf. Coat. Technol.* **1997**, *93*, 37–45. [CrossRef]
12. Zhao, X.; Zhang, X.; Yin, Z.W.; Li, W.J.; Yang, C.P.; Sun, W.H.; Zhang, H.L.; Li, Y. Enhanced Electrochromic Performance of All-Solid-State Electrochromic Device Based on W-Doped NiO Films. *Coatings* **2022**, *12*, 118. [CrossRef]

13. Mouratis, K.; Tudose, I.V.; Romanitan, C.; Pachiu, C.; Popescu, M.; Simistiras, G.; Couris, S.; Suchea, M.P.; Koudoumas, E. WO_3 Films Grown by Spray Pyrolysis for Smart Windows Applications. *Coatings* **2022**, *12*, 545. [CrossRef]

14. Kaklauskas, A.; Zavadskas, E.K.; Raslanas, S.; Ginevicius, R.; Komka, A.; Malinauskas, P. Selection of low-e windows in retrofit of public buildings by applying multiple criteria method COPRAS: A Lithuanian case. *Energy Build.* **2006**, *38*, 454–462. [CrossRef]

15. Yu, Q.Q.; Guo, M.; Xu, W.X.; Shi, X.D.; Ma, Y.; Yu, J.Y.; Ding, B. Spray-assembly of thermos plasmonic nanoparticles: A speed-up fabrication strategy for energy-saving smart windows. *Sol. Energy* **2022**, *238*, 9–16. [CrossRef]

16. Hsu, P.C.; Liu, X.G.; Liu, C.; Xie, X.; Lee, H.R.; Welch, A.J.; Zhao, T.; Cui, Y. Personal Thermal Management by Metallic Nanowire-Coated Textile. *Nano Lett.* **2015**, *15*, 365–371. [CrossRef]

17. Murphy, C.J.; Gole, A.M.; Hunyadi, S.E.; Orendorff, C.J. One-dimensional colloidal gold and silver nanostructures. *Inorg. Chem.* **2006**, *45*, 7544–7554. [CrossRef]

18. Lin, C.J.; Hur, J.; Chao, C.Y.H.; Liu, G.Z.; Yao, S.H.; Li, W.H.; Huang, B.L. All-weather thermochromic windows for synchronous solar and thermal radiation regulation. *Sci. Adv.* **2022**, *8*, 7359. [CrossRef]

19. Hanauer, S.; Celle, C.; Crivello, C.; Szambolics, H.; Munoz-Rojas, D.; Bellet, D.; Simonato, J.P. Transparent and Mechanically Resistant Silver-Nanowire-Based Low-Emissivity Coatings. *ACS Appl. Mater. Interfaces* **2021**, *13*, 21971–21978. [CrossRef]

20. Lin, S.; Wang, H.Y.; Zhang, X.N.; Wang, D.; Zu, D.; Song, J.A.; Liu, Z.L.; Huang, Y.; Huang, K.; Tao, N.A.; et al. Direct spray-coating of highly robust and transparent Ag nanowires for energy saving windows. *Nano Energy* **2019**, *62*, 111–116. [CrossRef]

21. Hu, H.B.; Wang, S.C.; Wang, S.C.; Liu, G.W.; Cao, T.; Long, Y. Aligned Silver Nanowires Enabled Highly Stretchable and Transparent Electrodes with Unusual Conductive Property. *Adv. Funct. Mater.* **2019**, *29*, 1902922. [CrossRef]

22. Johan, M.R.; Aznan, N.A.K.; Yee, S.T.; Ho, I.H.; Ooi, S.W.; Singho, N.D.; Aplop, F. Synthesis and Growth Mechanism of Silver Nanowires through Different Mediated Agents ($CuCl_2$ and NaCl) Polyol Process. *J. Nanomater.* **2014**, *2014*, 105454. [CrossRef]

23. Trung, T.N.; Arepalli, V.K.; Gudala, R.; Kim, E.T. Polyol synthesis of ultrathin and high-aspect-ratio Ag nanowires for transparent conductive films. *Mater. Lett.* **2017**, *194*, 66–69. [CrossRef]

24. Rui, Y.J.; Zhao, W.L.; Zhu, D.W.; Wang, H.Y.; Song, G.L.; Swihart, M.T.; Wan, N.; Gu, D.W.; Tang, X.B.; Yang, Y.; et al. Understanding the Effects of NaCl, NaBr and Their Mixtures on Silver Nanowire Nucleation and Growth in Terms of the Distribution of Electron Traps in Silver Halide Crystals. *Nanomaterials* **2018**, *8*, 161. [CrossRef] [PubMed]

25. Sun, Y.G.; Mayers, B.; Herricks, T.; Xia, Y.N. Polyol synthesis of uniform silver nanowires: A plausible growth mechanism and the supporting evidence. *Nano Lett.* **2003**, *3*, 955–960. [CrossRef]

26. Kottmann, J.P.; Martin, O.J.F.; Smith, D.R.; Schultz, S. Plasmon resonances of silver nanowires with a nonregular cross section. *Phys. Rev. B* **2001**, *64*, 235402. [CrossRef]

27. Mao, H.B.; Feng, J.Y.; Ma, X.; Wu, C.; Zhao, X.J. One-dimensional silver nanowires synthesized by self-seeding polyol process. *J. Nanopart. Res.* **2012**, *14*, 1–15. [CrossRef]

28. Jo, H.A.; Jang, H.W.; Hwang, B.Y.; Kim, Y.H.; Kim, J.Y. Synthesis of small diameter silver nanowires via a magnetic-ionic-liquid-assisted polyol process. *RSC Adv.* **2016**, *6*, 104273–104279. [CrossRef]